Mononuclear copper(II) complexes containing a macrocyclic ditopic ligand: synthesis, structures and properties

Massinissa Ayad, Philippe P. Schollhammer, Yves Le Mest, Laurianne Wojcik, François Pétillon, Nicolas Le Poul, Dominique Mandon

Mononuclear copper(II) complexes containing a macrocyclic ditopic ligand: synthesis, structures and properties.

Massinissa Ayad,[a] Philippe Schollhammer,[a] Yves Le Mest,[a] Laurianne Wojcik,[a]
François Y. Pétillon,[a,*] Nicolas Le Poul,[a,*] Dominique Mandon,[a, †]

[a] *UMR CNRS 6521, Laboratoire de Chimie, Electrochimie Moléculaires et Chimie Analytique, Université de Bretagne Occidentale, 6 Avenue Victor Le Gorgeu, CS 93837, 29238 Brest-Cedex 3, France*
Email : francois-yves.petillon@univ-brest.fr, nicolas.lepoul@univ-brest.fr

[†] Deceased in July 2016

KEYWORDS: Copper complexes; Nitrogen ligands; Macrocylic ligands; copper-hydroperoxo species ; hydrogen peroxide.

Abstract

Three different mononuclear copper(II) complexes **1-3** bearing ditopic macrocyclic ligands (**L**^{1} or **L**^{2}) have been prepared. Both ligands include two coordinating cores, namely tris(methylpyridyl)amine (TPA) and pyridine-dicarboxamide (PydCA). Complexes **1-3** have been characterized in solid state, and in solution by UV-Vis and EPR spectroscopies, as well as by cyclic voltammetry. X-ray diffraction analyses of crystals of complexes **1** and **3** show that the Cu(II) ion is preferably coordinated in the TPA site. Moreover, the coordination sphere of the copper center fully depends on the Cu(II) salt used for the synthesis ($CuCl_2$ for **1** and **2**, $Cu(OTf)_2$ for **3**). Hence, the tetracoordinated bis-chloro complex **1** adopts a distorted square-planar geometry at solid state, whereas the pentacoordinated bis-aqua complex **3** displays an almost perfect square pyramidal conformation. Both complexes **1** and **3** react with H_2O_2 in acetonitrile, leading to the formation of copper(II)-hydroperoxo species according to the UV-Vis spectroscopic studies.

1. Introduction

Iron and copper hydroperoxide complexes have been well investigated over the past 30 years, because these adducts are reactive intermediates for many biological and chemical oxidation processes [1-3]. In particular, $[Cu\text{-}OOH]^{n+}$ (n = 1, 2) species have been proposed as being key intermediates involved in proton-coupled electron transfer (PCET) reactions promoted by monooxygenase enzymes, such as peptidylglycine α-hydroxylating monooxygenase (PHM) [4-

6], lytic polysaccharide monooxygenase (LPMO) [7], or galactose oxidase (GO) [8]. Most of the reported biomimetic copper(II) hydroperoxide complexes have been shown to be unstable at room temperature [9-21]. These species are usually prepared upon reaction of a Cu(II) complex with H_2O_2 in presence of a base (NEt_3). Reactivity of copper-hydroperoxo complexes was shown to be highly dependent on the mono- or dinucleating topology of the ligand, as well as its electronic and steric properties, which globally affect the O-O bond strength. For example, μ-1,1-hydroperoxo dicopper(II) complexes are electrophilic and typically allow O-transfer to nucleophilic substrates such as PPh_3, but cannot perform H-atom abstraction [21]. In contrast, some mononuclear copper-hydroperoxo complexes were shown to be able to oxidize heterogeneous aromatic hydrocarbons, such as toluene or xylene [20]. Intramolecular aromatic hydroxylation and oxidative N-dealkylation of the supporting ligands have been also reported [15, 16]. Hence, the full control of the ligand architecture is crucial to afford the characterization and studies of copper hydroperoxide complexes, as regards to their potential employment in catalytic systems.

We have recently developed a macrocyclic ligand $\mathbf{L^1}$ (Scheme 1) which displays two coordinating sites (tris(methylpyridyl)amine (TPA), and pyridine-dicarboxamide (PydCA)) for metal ions attack [22]. This dissymmetrical ditopic ligand allows the generation of mono and dinuclear complexes. Our preliminary investigations were focused on mononuclear iron(II) complexes. Solid-state and solution studies demonstrated that the Fe(II) metal ion was coordinated in the TPA site. Reactivity of the complexes with H_2O_2 in the absence of an exogenous substrate leads to an intramolecular aromatic hydroxylation. Notably, catalytic studies for the oxidation of cyclohexane into cyclohexanone and cyclohexanol show that the macrocyclic topology of the ligand and the nature of the counter-ion strongly impacted the turn-over number through different reaction mechanisms.

From these results, we present here the synthesis and characterization of three new mononuclear Cu^{II}-($\mathbf{L}^n$) (n = 1, 2) complexes. Our aim was principally to rationalize the influence of the macrocyclic (rigid) structure of the ligands $\mathbf{L^1}$ and $\mathbf{L^2}$ (Scheme 1) on their structural, spectroscopic and electrochemical properties, in comparison to those of analogous copper complexes. The ligand $\mathbf{L^2}$ bearing an isobutyl group was synthesized in order to enhance the solubility of the neutral copper complex [23]. Moreover, we have investigated the impact of the counter-ion (Cl^- or OTf^-), used in the synthesis on the spectroscopic and crystallographic features, as well as on their reactivity towards hydrogen peroxide to generate stable copper-hydroperoxo species.

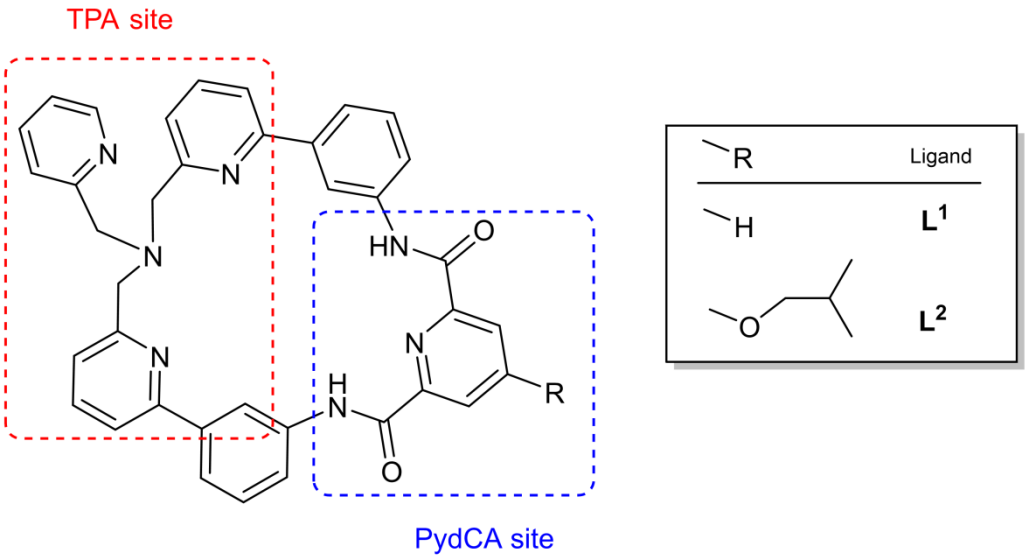

Scheme 1. Macrocylic and ditopic ligands $\mathbf{L^1}$ and $\mathbf{L^2}$.

2. Experimental

2.1 General Procedures

All air sensitive organic reactions, as well as the handling and synthesis of copper complexes were routinely carried out under an argon atmosphere using standard Schlenk techniques. Further manipulations were performed in MBraun UNILab sp glovebox workstation under an argon atmosphere. All chemicals were purchased from Sigma-Aldrich and used without purification. Solvents were either distilled immediately before use under nitrogen from appropriate drying agents or passed through MBraun MB SPS6800 solvent purification system. All dry solvents were degassed before use by bubbling N_2 through the liquid for 30 minutes or by freeze-thawing with nitrogen liquid under strict anaerobic conditions. CH_2Cl_2 used for electrochemistry was freshly distilled from CaH_2 and kept under Ar in the glovebox. IR spectra were recorded on a Bruker-Vertex 70-Avatar spectrometer from solids. Chemical analyses were performed by the "Service de Microanalyse" ICSN-CNRS of Gif/Yvette (France). The UV-Vis measurements were carried out on a Jasco V-650 (190-10000 nm) spectrophotometer or a Varian Cary 05 E UV-Vis spectrophotometer equipped with an Oxford instrument DN 1704 cryostat in optically transparent Schlenk cells; HPLC-grade acetonitrile was degassed under argon and stored in a glove box. NMR spectra were recorded in $CDCl_3$ at ambient temperature on a Bruker AC 400 (^1H, ^{13}C) spectrometer. EPR spectra were obtained from a Bruker Elexsys E500 spectrometer, at a perpendicular mode X band (9.36 GHz); simulations were performed using the Bruker X-Sophe software. Electrochemical studies of the complexes were performed in a glove box (Jacomex) (O_2 <1 ppm, H_2O <1 ppm) with a home-designed 3-electrode-cell (WE: glassy carbon, RE: Pt wire in a Fc^+/Fc solution, CE: Pt or a graphite rod). Ferrocene (Fc) was added at the

end of the experiments to determine redox potential values. The potential of the cell was controlled by using an AUTOLAB PGSTAT 100 (Metrohm) potentiostat monitored by the NOVA software. The supporting salt NBu_4PF_6 was synthesized from NBu_4OH (Acros) and HPF_6 (Aldrich), then it was purified, dried under vacuum for 48 hours at 100°C, and finally kept under argon in a glovebox. Mass spectrometric measurements were performed on an Autoflex MALDI TOF III LRF 200 spectrometer by the "Service Commun de Spectrométrie de masse" of the Université de Bretagne Occidentale (Brest).

2.2 Syntheses of the ligands

The ligand $\mathbf{L^1}$ was synthesized and characterized previously by us [22], according to a slight modified method of the literature [23]. The synthesis of $\mathbf{L^2}$ was performed similarly to that of the cyclo [bis((3-(pyridine-2-yl)-5-phenyl-2,6-dicarboxamide)amine] 2-pyridylmethyl ($\mathbf{L^1}$) [24]. After the required purification steps the ligand was obtained as a pure, light-brown powder in valuable yields (62%).

Data for $\mathbf{L^2}$: IR (solid, cm^{-1}): ν(NH) 3313 (w), ν(C=O) 1681 (m). ^{1}H NMR (400 MHz, $CDCl_3$): δ 10.52 (s, 2H), 8.59 (d, *J* = 7.6 Hz, 1H), 8.33 (d, *J* = 4.4 Hz, 1H), 8.13 (s, 2H), 7.99 (s, 2H), 7.67 (t, *J* = 7.6 Hz, 4H), 7.50 (m, 8H), 7.31 (d, *J* = 7.0 Hz, 1H), 6.95 (t, *J* = 5.8 Hz, 1H), 4.12 (s, 4H), 4.07 (s, 2H), 3.95 (d, *J* = 6.4 Hz, 2H), 2.18 (m, 1H), 1.07 (d, *J* = 6.4 Hz, 6H). ^{13}C NMR (125.72 MHz, $CDCl_3$): δ 190.0 (2C, **C**H_3, ^{i}OBut), 168.3, 161.7, 158.4, 151.0, 140.3, 138.4 (12C, $\mathbf{C}_{ipso}$), 157.1 (2C, **C**=O), 137.3, 132.2, 132.1, 131.9, 129.5, 128.6, 128.5, 123.0, 122.8, 121.8, 120.9, 119.8, 119.0, 112.0 (20 **C**H), 75.3 (**C**H_2, ^{i}OBut), 61.5 (2C, N-**C**H_2-Py), 59.4 (1C, N-**C**H_2-Py). MS ($CHCl_3$, m/z): Calcd for [M]: 675.29 (100%). Found: 674.4 for [M-H].

2.3 Syntheses of the Cu(II) complexes

*[$CuCl_2$($\mathbf{L^1}$)] (**1**)*

To a THF (10 mL) solution of $\mathbf{L^1}$ (50 mg, 0.08 mmol) in a Schlenk tube was added a blue solution of $CuCl_2$ (11.2 mg, 0.08 mmol) in THF (10 mL). Upon addition, the solution colored to green. The mixture was stirred for 8h at room temperature and then filtered. The resulting solution was concentrated by evaporation of the solvent, and Et_2O (30 mL) was added to precipitate the product, that was washed with Et_2O (2x5 mL) and dried *in vacuum* to yield the product **1** as a green solid. Yield: 46 mg, 78%. Blue crystals suitable for an X-ray analysis were obtained, at room temperature, by slow vapor diffusion of diethyl ether into a CH_3CN solution of **1**. IR (solid, cm^{-1}): ν(NH) 3300 (w), ν(CO) 1679 (m). UV-Vis (MeCN) λ_{max}, nm (ε, $M^{-1}cm^{-1}$): 261 (29990), 284 (28080), 646 (23), ESI-MS [$CH_3CN/CHCl_3$ (1/9)] found (calcd) for $[M\text{-}2Cl]^+$ *m/z*: 666.86 (666.86). EPR (9.32 GHz; CH_2Cl_2; 150 K): g// = 2.14, g⊥ = 2.08, A// = 171 G. Elemental analysis calcd (%) for $C_{37}H_{29}Cl_2CuN_7O_2$. $3H_2O$: C, 56.08; H, 4.45; N, 12.38. Found: C, 55.06; H 4.03; N, 10.80.

*[$CuCl_2$(**L**^{2})] (**2**)*

Similarly, a blue solution of $CuCl_2$ (18.9 mg, 0.14 mmol) in dry THF (5 mL) was added to a brown solution of **L**^{2} (100 mg, 0.14 mmol) in THF (5mL) at room temperature; upon addition the solution colored to blue. The reaction mixture was stirred overnight, after which time diethyl ether (50 mL) was added to precipitate the product. The supernatant was removed *via* cannula filtration and the product was washed with Et_2O (3x15 mL), dried *in vacuum*, giving **2** as a blue-green powder. Yield 64 mg, 56%. In spite of several attempts no crystal of **2** suitable for X-ray analysis was obtained. IR (solid, cm^{-1}): ν(NH) 3322 (w), ν(CO) 1675 (m). UV-Vis (MeCN) λ_{max}, nm (ε, $M^{-1}cm^{-1}$): 258 (22460). 302 (18630), ESI-MS ($CHCl_3$) found (calcd) for $[M\text{-}2Cl]^+$ m/z: 738.38 (738.22). EPR (9.30 GHz; CH_3CN; 150 K): g// = 2.22, g⊥ = 2.05, A// = 164 G.

*[$Cu(H_2O)_2$(**L**^{1})]$(OTf)_2$, H_2O (**3**)*

To a yellow-brown solution of **L**^{1} (60 mg, 0.09 mmol) in THF (3 mL) was added a blue solution of [$Cu(OTf)_2$] (36 mg, 0.09 mmol) at room temperature. Upon addition the solution colored to dark green. The mixture solution was stirred for 8h and after filtered, 20 mL of diethyl ether were then added to the filtrate to precipitate a green solid. The solvents were removed by filtration and the residue was washed with ether (3x5 mL) and dried in *vacuum* to yield product **3** as a blue-green powder. The formulation of **3** was deduced from elemental analysis as being [$Cu(H_2O)_2$(**L**^{1})]$(OTf)_2$, H_2O. Yield: 50 mg, 56%. Crystals suitable for a X-ray diffraction study were obtained by slow vapor diffusion of Et_2O into a CH_3CN solution of **3** in a sealed tube. IR (solid, cm^{-1}): ν(NH) 3334 (w), ν(CO) 1654 (w), ν(CF) 1027 (s). UV-Vis (MeCN) λ_{max}, nm (ε, $M^{-1}cm^{-1}$): 257 (28110), 284 (26400), 666 (51), EPR (9.30 GHz; CH_3CN; 150 K): g// = 2.27, g⊥ = 2.05, A// = 166 G. Elemental analysis calcd (%) for $C_{39}H_{29}CuF_6N_7O_8S_2$. 1 H_2O: C, 45.93; H, 3.46; N, 9.62. Found: C, 45.72; H, 3.17; N, 9.23.

2.4 X-ray structural determination

Measurements for compounds **1** and **3** were made on an Oxford Diffraction X-Calibur-2CDD diffractometer equipped with a jet cooler device. Graphite-monochromated Mo Kα radiation (λ = 0.71073 Å) was used in all experiments. The structures were solved and refined by standard procedures [25, 26]. A nitrogen stream cryostat attached to the system enabled low-temperature measurements (170K). Intensity data were collected combining several runs (omega-scan, step 1°) in order to obtain a complete set of reflections (as far as possible down to *d* = 0.8 Å or less). Bond lengths, angles, data collection and processing parameters are given in Table 1 and in the SI.

Table 1. Crystallographic data and refinement parameters of the complexes **1** and **3**.

	1	**3**
Empirical formula	$C_{41}H_{35}Cl_2CuN_9O_2$	$C_{82}H_{76}Cu_2F_{12}N_{14}O_{21}S_4$
Formula weight	820.22	2076.89
Temperature (°K)	170(2)	170(2)
Wavelength (Å)	0.71073	0.71073
Crystal system, space group	Monoclinic, P1 21/c1	Monoclinic, P1 21/n 1
Unit cell dimensions : a (Å)	13.2568(6)	11.3061(3)
b (Å)	21.6185(7)	18.4544(5)
c (Å)	14.3023(6)	21.4444(5)
β(°)	114.1535(5)	97.720(2)
Volume ($Å^3$)	3740.1(3)	4433.8(2)
Z	4	2
D(calc) (Mg m^{-3})	1.457	1.556
Absorption coefficient (mm^{-1})	0.778	0.679
F(000)	1692	2128
Crystal description	Flat spindle-shape needle	Prism, axis [ ] ?
Crystal color	Clear light green	Light blue
Crystal size (mm)	0.46x0.35x0.04	0.44x0.24x0.08
Theta range for data collection (°)	3.44 to 26.37	3.38 to 26.37
Limiting indices	-16≤ h ≤14, -26≤ k ≤27, -17≤ l ≤17	-13≤ h ≤14, -23≤ k ≤23, -25≤ l ≤26
Reflections collected/unique	23102/7627 [R(int) = 0.0545]	39084/9050 [R(int) = 0.0619]
Completeness to theta = 26.37(%)	99.7	99.8
Absorption correction	Semi-empirical from equivalents	Analytical
Max. and min. transmission	0.9696 and 0.7162	0.9477 and 0.7543
Refinement method	Full-matrix least-squares on F^2	Full-matrix least-squares on F^2
Data/restraints/parameters	11513/24/493	9050/60/654
Goodness of fit on F^2	1.027	1.041
Final R indices [I>2σ(I)]	R_1 = 0.0452, wR_2 = 0.1031	R_1 = 0.0453, wR_2 = 0.1042
R indices (all data)	R_1 = 0.0694, wR_2 = 0.1155	R_1 = 0.0606, wR_2 = 0.1124
Largest diff. peak and hole ($eÅ^{-3}$)	0.856 and -0.523	0.687 and -0.864

3. Results and discussion

3.1 Syntheses and characterization of the ligands

The ligand $\mathbf{L^1}$ has been synthesized previously [22]. The synthesis of $\mathbf{L^2}$ was performed similarly to that of $\mathbf{L^1}$. $\mathbf{L^2}$ was obtained as a light-brown powder in valuable yields (62%), by adding a tetrahydrofuran solution of 4-isobutylether-2,6-dicarbonyldichloride-pyridine, instead of 2,6-pyridine bicarbonylchloride to a tetrahydrofuran/acetonitrile solution of 2-aminophenyl-6-methylpyridine used for $\mathbf{L^1}$, as described in Scheme 2. $\mathbf{L^2}$ was characterized by spectroscopy (see the Experimental part), and its geometry was confirmed by an X-ray diffraction study [24].

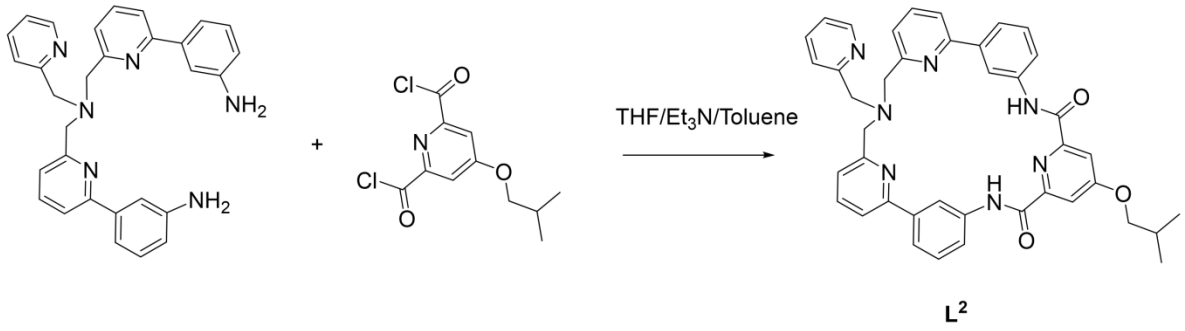

Scheme 2. Synthetic pathway for $\mathbf{L^2}$

3.2 Syntheses and spectroscopic characterization of the Cu^{II} complexes

The synthetic procedure to prepare the mononuclear complexes **1-3** is identical to that described for analogous iron(II) complexes [22] (Scheme 3). The metalation proceeds by addition of stoichiometric amounts of the metal salt, $CuCl_2$ or $[Cu(OTf)_2]$, to a THF solution of the ligand $\mathbf{L^n}$ (n = 1, 2), without the addition of a base. The complexes are obtained as green or blue-green powders in noticeable yields (see the Experimental part). Elemental analysis suggests that the complex **1** contains three solvate water molecules and was formulated as $[CuCl_2(\mathbf{L^1})]$**.**$3H_2O$; the water molecules probably arise from the use of wet solvents. Such a structure was confirmed by an X-ray diffraction study of crystals of **1** (see below; Figure 1), obtained by slow diffusion of diethyl ether into a CH_3CN solution of **1**, but with two molecules of acetonitrile as solvate instead of 3 H_2O. ESI-MS accords with the formulation [M-2Cl], with M = {Cu($\mathbf{L^1}$)}. In spite of several attempts no reproducible result was obtained for elemental analysis of **2**, probably because some instability of the product. Therefore, complex **2** was only characterized by spectroscopy. The similarities of their spectroscopic data suggest that **2** and **1** have also similar geometry.

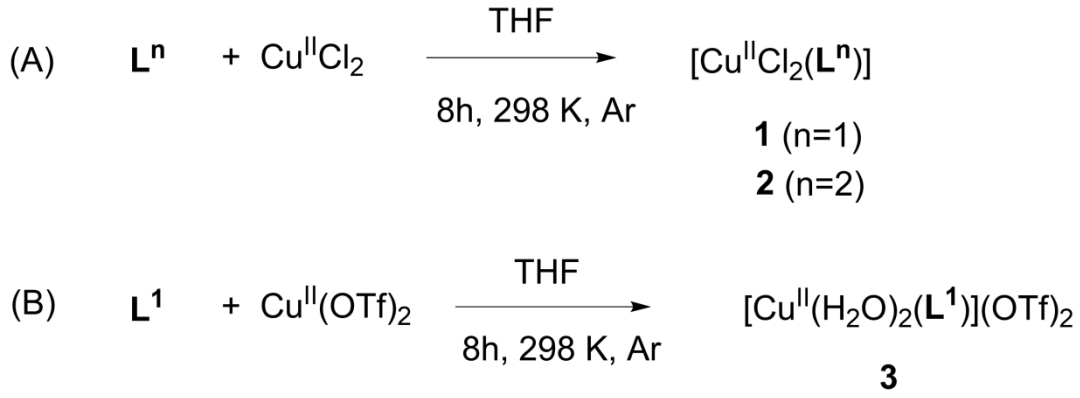

Scheme 3. The synthetic pathways for the complexes **1** and **2** (path A), and **3** (path B).

The formulation of **3** was deduced from elemental analysis as being the dicationic compound $[Cu(H_2O)_2(\mathbf{L^1})](OTf)_2.H_2O$, which contains a solvate water molecule. This structure was confirmed by an X-ray diffraction study of crystals of the complex (see below; Figure 2), obtained by slow diffusion of diethyl ether into an acetonitrile solution of **3** with, however, the presence of a half molecule of diethyl ether, instead of 1 H_2O.

The infrared spectra of complexes **1**-**3** display two main bands near 3300 and 1660 cm^{-1}, which can be assigned, respectively, to the vibrations of the NH and CO bonds of the uncoordinated imide moieties. These frequency values are close to those observed for the free ligands $\mathbf{L^1}$ and $\mathbf{L^2}$ (ν = 3313, and 1681 cm^{-1}); these results are in agreement with the crystallographic data, which show complexation on the TPA site. The other spectroscopic data (UV-vis, EPR), ESI-MS and the molar conductivity accord also with the structures proposed for complexes **1**-**3** (see the Experimental part, and below). In particular, mass spectroscopy of complex **1** into a mixture of $CHCl_3/CH_3CN$ (9:1) shows the presence of a peak at m/z = 666.86, which corresponds to the monocationic complex **1** deprived of the chloride ions, namely $[Cu(\mathbf{L^1})]^+$. Hence, it should be concluded to the decoordination of both chloride anions occurs in these experimental conditions.

*3.3 X-ray diffraction study of **1** and **3***

The crystal structure of **1** is shown in Figure 1. Selected bond lengths and angles are gathered in Table 2 (see SI for further details). The structural analysis reveals that crystals of **1** were formed with two solvate molecules of acetonitrile, and therefore this compound was formulated in the solid state as $[CuCl_2(\mathbf{L^1})]$. 2 CH_3CN. The Cu(II) ion is tetra-coordinated by two chlorides and a bidentate N-donor ligand fragment, involving the TPA site; precisely, the nitrogen atoms are those of the tertiary amine (N(1)) and the unsubstituted pyridine (N(7)). The geometry can be considered as a distorted square-plane. For the nitrogen atoms N(2) and N(6) of the substituted pyridyl groups of the TPA ligand, the copper-nitrogen distances are long (Cu(1)-N ~ 2.91 Å) compared to the Cu(1)–N(1) and Cu(1)-N(7) ones (Cu(1)-N ~2.06 Å), suggesting at the most weak metal-ligand interaction. The dihedral angle ω between the two plans defined by the Cl(1)-Cu(1)-N(1) and Cl(2)-Cu(1)-N(7) atoms equals 15.20°, which indicates that the square-plane is slightly distorted [27]. The chloride ion (Cl(1)) in the proximity of the amide groups is at ~ 2.5 Å from the most proximal atoms (Table 3), which suggests only a light hydrogen-bonding stabilization.

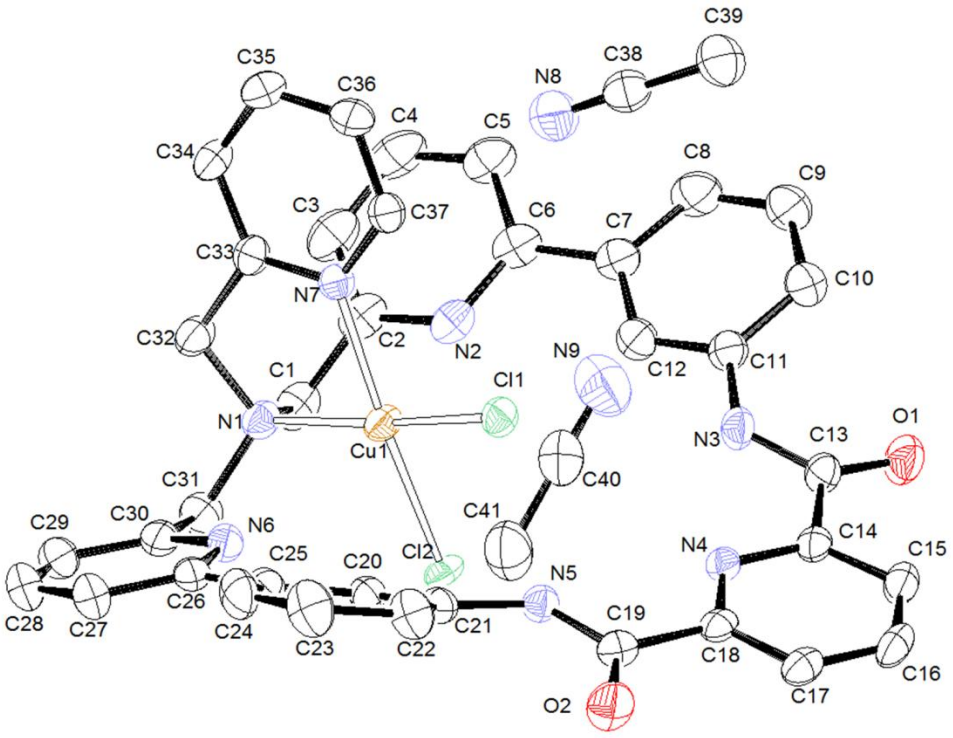

Figure 1. Molecular structure of **1** (thermal ellipsoids at 50% level). The hydrogen atoms are not displayed for clarity.

The solid-state structure of complex **1** is radically different from that of its analogous complex $[CuCl(TPA)]^+$. Indeed, the latter displays a pentacoordinated copper ion in a bipyramid trigonal geometry, including four nitrogen atoms (Cu-N average distance: 2.06 Å) [28]. Such a discrepancy at solid state might be correlated to the rigidity of the ligand $\mathbf{L^1}$ which does not allow coordination of all nitrogen atoms of the TPA core. Here, this lack of flexibility is compensated by the presence of a second chloride anion in the first coordination sphere.

Table 2. Selected bond lengths (Å) and angles (°) for complexes **1** and **3**.

Compound 1				
	N(1)-Cu(1)	2.085(2)	N(7)-Cu(1)-N(1)	82.28(9)
	N(7)-Cu(1)	2.033(2)	N(7)-Cu(1)-Cl(1)	91.98(7)
	Cl(1)-Cu(1)	2.2619(7)	N(7)-Cu(1)-Cl(2)	169.57(7)
	Cl(2)-Cu(1)	2.3020(7)	N(1)-Cu(1)-Cl(1)	171.67(7)
			N(1)-Cu(1)-Cl(2)	94.15(7)
			Cl(1)-Cu(1)-Cl(2)	92.52(3)

Solvate (CH_3CN**)**				
	C(38)-C(39)	1.459(5)	C(39)-C(38)-N(8)	178.9(4)
	C(38)-N(8)	1.131(4)	C(41)-C(40)-N(9)	179.3(4)
	C(40)-C(41)	1.450(5)		
	C(40)-N(9)	1.137(5)		

Compound 3			
Cation			
N(1)-Cu(1)	2.044(2)	N(1)-Cu(1)-N(7)	82.30(8)
N(6)-Cu(1)	2.039(2)	N(1)-Cu(1)-N(6)	83.08(8)
N(7)-Cu(1)	2.011(2)	N(1)-Cu(1)-O(1)	162.29(8)
O(1)-Cu(1)	1.986(2)	N(1)-Cu(1)-O(2)	101.47(8)
O(2)-Cu(1)	2.161(2)	N(6)-Cu(1)-N(7)	165.02(9)
O(1/2)-H(1/2v)	~0.845(23)	N(6)-Cu(1)-O(1)	96.34(8)
O(1/2)-H(1/2w)	~0.846(23)	N(6)-Cu(1)-O(2)	95.17(8)
N(3)-H(3_N)	0.851(21)	N(7)-Cu(1)-O(1)	96.60(8)
N(5)-H(5_N)	0.866(20)	N(7)-Cu(1)-O(2)	90.90(8)
		O(1)-Cu(1)-O(2)	96.22(8)
		H(1/2v)-O(1/2)-H(1/2w)	~108(3)
		Cu(1)-O(1)-H(1v/w)	117(2)
		Cu(1)-O(2)-H(2v/w)	113(2)
Anion			
S(1)-O(5-7)	~1.436	O(5-7)-S(1)-C(38)	~103.55(17)
S(1)-C(38)	1.832(4)	O(8-10)-S(2)-C(39)	~115.06(13)
C(38)-F(1-3)	~1.318(6)	F(1-3)-C(38)-S(1)	~110.9(3)
S(2)-O(8-10)	~1.435(2)	F(4-6)-C(39)-S(2)	~111.30(26)
S(2)-C(39)	1.817(4)	F-C(38)-F	~108.0(4)
C(39)-F(4-6)	~1.327(6)	F-C(39)-F	107.58(36)
Solvate (Et2O)			
C(40)-C(41)	1.481(12)	C(42)-O(11)-C(40)	115.6(8)
C(40)-O(11)	1.414(10)		
C(42)-C(43)	1.492(16)		
C(42)-O(11)	1.391(12)		

Monocrystals of **3** have been obtained by slow diffusion of diethyl ether in an acetonitrile solution of the complex in a sealed tube. Crystals of **3** have been analyzed by X-ray diffraction. According to this analysis, complex **3** crystallizes as $[Cu(H_2O)_2(\mathbf{L})][OTf]_2.0.5\ Et_2O$. X-ray structure of **3** (Figure 2) reveals the presence of two mononuclear complexes in the unit cell, but crystallographically distinct Cu(II) centers (Table 1 and SI). Each copper(II) ion is pentacoordinated in the TPA site of the $\mathbf{L}^2$ ligand, within a pseudo-square-based pyramidal geometry including the (O(1), N(1), N(6), N(7)) square and the apical O(2) atom. The value of Addison parameter τ for this structure (τ=0.05) indicates an almost perfect square pyramidal geometry of the first coordination sphere of the metal ion. As shown in Table 2, the shorter Cu(1)-O(1) bond length (vs Cu(1)-O(2)) can be ascribed to a trans-effect of the nitrogen atom N(1) in the equatorial plan.

The bond lengths for the solvate in **1** (CH_3CN) and **3** (Et_2O) are those expected for such a non-bonded molecule. In other respects, the structural analysis reveals that, by coordination to Cu(II) ion, the macrocycle $\mathbf{L}^1$ is much more distorted in **3** than in **1**.

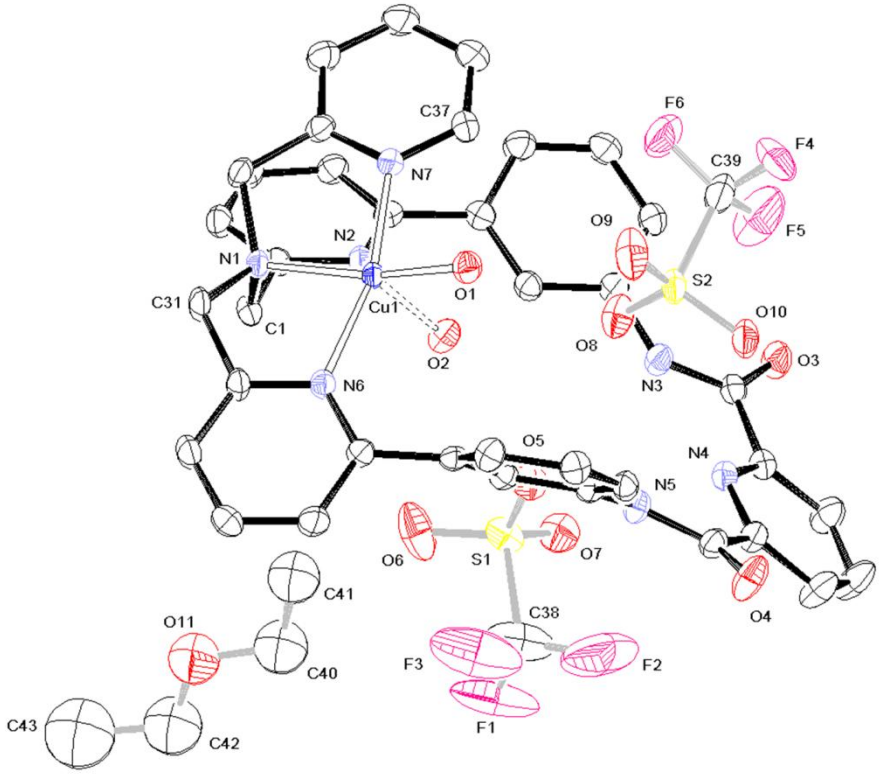

Figure 2. Molecular structure of **3** (thermal ellipsoids at 50% level). The hydrogen atoms are not displayed for clarity.

Table 3. D-H..A distances (Å) and angles (°) in **1** and **3**.

D-H¨A	d(N-H)	D(H¨A)	d(N¨A)	D(D-H¨A)
Compound 1				
N(3)-H(3N).Cl(1)	0.871(14)	2.571(15)	3.375(2)	154.0(15)
N(5)-H(5N).Cl(1)	0.874(14)	2.476(16)	3.248(2)	147.7(16)
Compound 3				
N(3)-H(3N).O(5)	0.850(17)	2.37(2)	3.135(3)	149(2)
N(3)-H(3N).O(8)	0.850(17)	2.60(2)	3.123(3)	121(2)
N(5)-H(5N).O(5)	0.866(17)	2.219(19)	3.033(3)	156(2)
N(5)-H(5N).O(8)	0.866(17)	2.73(2)	3.158(3)	112.1(2)

As shown in Table 3, there is no interaction in complex **1** between the chlorine and ligand hydrogen (**H**-N(3/5)) atoms (H¨Cl~2.52 Å). Similarly, no obvious interaction is detected in complex **3** between oxygen atoms (O (5/8)) of the solvate and amine hydrogens of the TPA ligand (H-N(3/5)), with the average "O¨H" distance of 2.48 Å. However, a weak interaction can be observed in **3** between the hydrogens of the two bound water molecules (**H**-O(1/2)) and oxygen atoms of the two solvate molecules (d(O-H)~1.90 Å); a weak interaction is also detected between the TPA nitrogen atom, N(2), and the hydrogen of a water molecule (d(N-H(2v)~1.93 Å) (see SI).

3.4 EPR spectroscopic studies

EPR spectroscopy of complexes **1** and **3** was recorded in frozen dichloromethane and acetonitrile (T = 155 K). All Cu(II) complexes display an anisotropic spectrum with similar features, except for complex **1** in CH_2Cl_2. Simulation of the spectra led to the determination of the g and A parameters. (see Table 4 and SI). The values obtained for complex **1** in CH_3CN, and complex **3** in both solvents ($g_{//}$ = 2.24-2.26; $g_{\perp}$ = 2.06-2.08; $A_{//}$ = 166 10^{-4} cm^{-1}) are typical of a penta-coordinated copper(II) complex in a square-pyramidal geometry [29]. The complex **3** seems poorly affected by the change of solvent, indicating that substitution of H_2O by CH_3CN does not modify the coordination sphere of the copper(II) ion. This is in agreement with solid state data showing a nearly perfect square-pyramidal conformation in which water molecules can be easily substituted (*vide supra*). The effect of solvent was however more important for complex **1**, since a rhombic signal (g_1 = 2.06 (A_1 = 30 10^{-4} cm^{-1}), g_2 = 2.08 (A_2 = 35 10^{-4} cm^{-1}), g_3 = 2.24 (A_3 = 160 10^{-4} cm^{-1})) was obtained for the complex in dichloromethane, whereas an axial signature was detected in acetonitrile. Again, these results are consistent with X-ray data. Probably, the complex remains in the pseudo-axial conformation in CH_2Cl_2, as in solid state, but undergoes substitution of chloride ions by nitrilo ligands in acetonitrile.

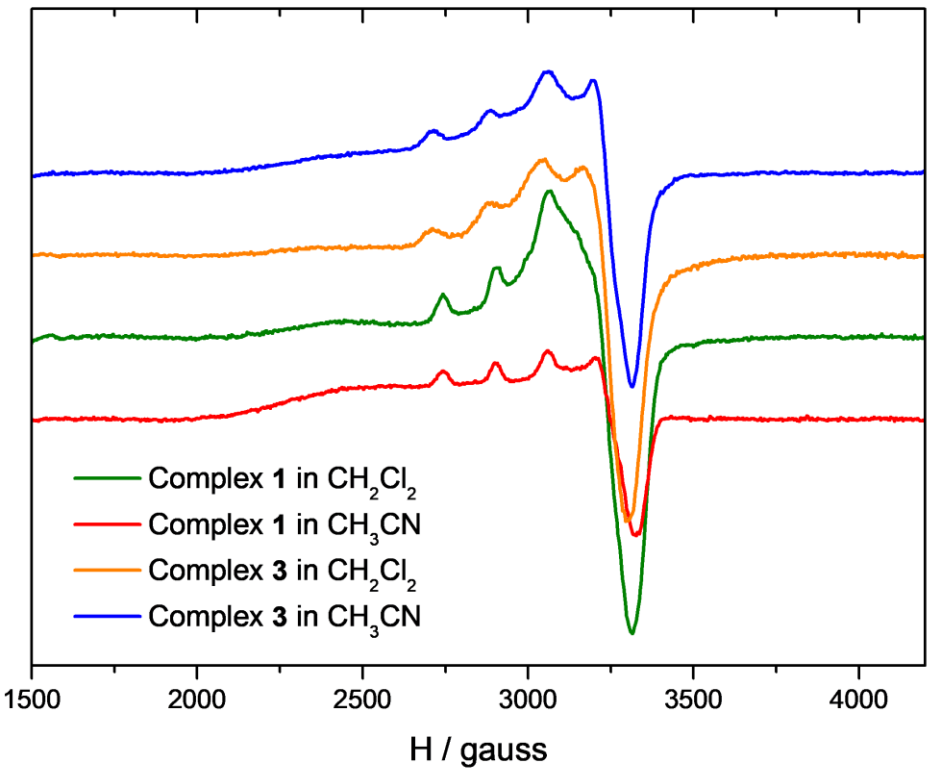

Figure 3. EPR spectra of complexes **1** (green: CH_2Cl_2; red: CH_3CN) and **3** (orange: CH_2Cl_2; blue: CH_3CN) at *T*=155 K in frozen solutions of solvents.

Table 4. EPR data for complexes **1** and **3** in CH_2Cl_2 and CH_3CN.

	Complex **1**	Complex **3**
CH_2Cl_2	g_1 = 2.06 (A_1 = 30 cm^{-1})	$g_{//}$ = 2.26 ($A_{//}$ = 166 cm^{-1})
	g_2 = 2.08 (A_2 = 35 cm^{-1})	$g_{\perp}$ = 2.08
	g_3 = 2.24 (A_3 = 160 cm^{-1})	
CH_3CN	$g_{//}$ = 2.24 ($A_{//}$ = 166 cm^{-1})	$g_{//}$ = 2.26 ($A_{//}$ = 166 cm^{-1})
	$g_{\perp}$ = 2.06	$g_{\perp}$ = 2.08

3.5 UV-Vis spectroscopic studies.

The UV-Vis studies showed that complexes **1** and **3** displayed similar spectroscopic signatures in acetonitrile (see Supplementary Information for spectra). Two intense bands located at 284-285 nm and 261 nm were detected, corresponding to $\pi \rightarrow \pi^*$ transition in the pyridine ligand and phenyl groups, respectively (for comparison the ligand $\mathbf{L^1}$ displayed two bands at 288 nm and 250 nm). Complexes **1** and **3** also showed a low absorption band in the visible region (λ_{max} = 646 nm and 666 nm, respectively), which can be ascribed to a d-d electronic transition. These values are in the same

range of those found for analogous penta-coordinated copper bis-pyridyl-amine complexes developed by Itoh *et al* [30].

3.6 Voltammetric studies.

Comparative voltammetric studies of complexes **1** and **3** were carried out in CH_2Cl_2 / NBu_4PF_6 0.1 M at a platinum working electrode. For both complexes, an irreversible peak was detected upon reduction on scanning negatively (Figure 4). The value of this reduction peak was found to be slightly more negative for **1** than for **3** (-0.72 V and -0.55 V vs. Fc, respectively), and is in the same range, for complex **1**, as previously reported for $[CuCl(TPA)]^+$ in CH_2Cl_2 (-0.75 V vs. Fc) [31]. This redox process is ascribed to the monoelectronic reduction of the Cu(II) into Cu(I). Cycling back led to the appearance of one or several oxidation peaks depending on the complex and the scan rate. The large peak separation between oxidation and reduction peaks is typical of copper complexes with strong rearrangement of the coordination sphere upon electron transfer [32]. This effect is associated with the different coordination and geometric properties between Cu(II) and Cu(I) redox states. Thus, the reduction at $E_{pc}(1)$ generates a Cu(I) unstable species that evolves into a copper complex by probable unbinding of one ligand.

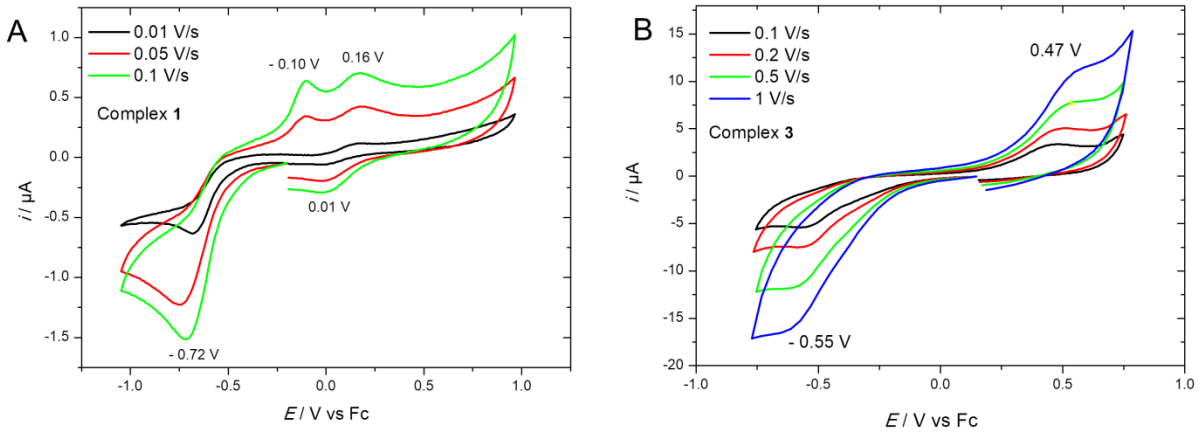

Figure 4. Cyclic voltammograms of complexes **1** (A) and **3** (B) at a Pt working electrode in CH_2Cl_2/NBu_4PF_6 0.1 M at different scan rates. *E* /V vs. Fc.

*3.7 Reactivity of complexes **1** and **3** towards H_2O_2.*

The reaction of complex **1** and **3** with H_2O_2 in acetonitrile at room temperature was monitored by UV-Vis spectroscopy (see Figure 5). Both experiments clearly show that the complexes evolve towards a new species which displays an absorption band at λ_{max} = 387 nm. The wavelength value is close to that obtained for analogous copper-hydroperoxo complexes such as $[Cu^{II}(BPPA)(OOH^-)]^+$ (380 nm)[10] and $[Cu^{II}(TPA)(OOH^-)]^+$ (379 nm) [33]. The absorption bands are assigned to a Ligand to Metal Charge Tranfser (LMCT) from the hydroperoxide ligand to the Cu(II) ion. Hence, these results suggest

here the formation of the complex $[Cu^{II}(\mathbf{L^1})(OOH^-)]^+$ from both complexes **1** and **3** (Scheme 4). This indicates that the reaction with H_2O_2 induced the unbinding of chloride and water ligand from the copper center. As shown in Figure 5, the formation of the hydroperoxo complex is slow at room temperature, the generated species being stable over several hours. Possibly, the Cu-OOH complex is stabilized through weak interactions (H-bonding) with the second coordinating core (PydCA).

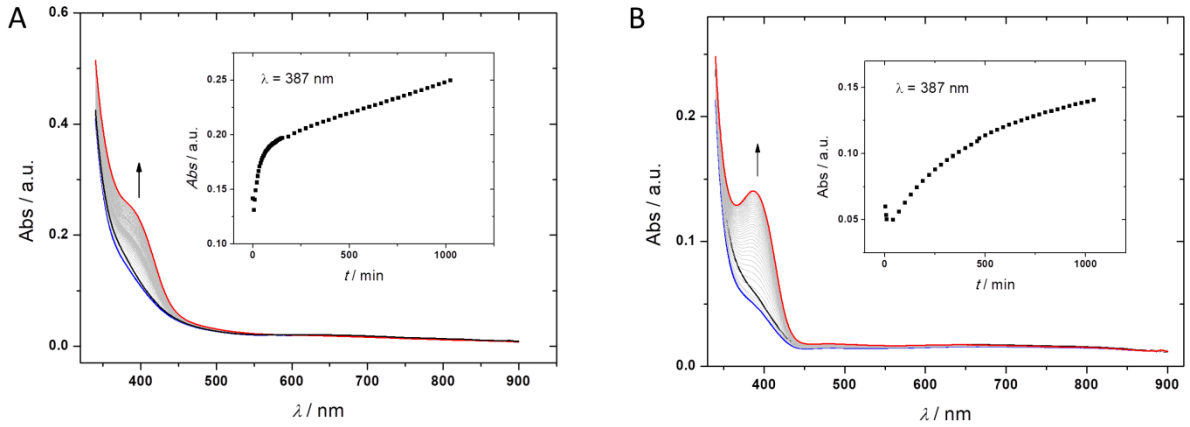

Figure 5. UV-Visible spectroscopic monitoring of the reaction in CH_3CN of A) complex **1** (3 mM) with H_2O_2 (30 mM), and B) complex **3** (5 mM) with H_2O_2 (15 mM) at room temperature. Inset: Plots of Abs(387 nm) *vs*. time.

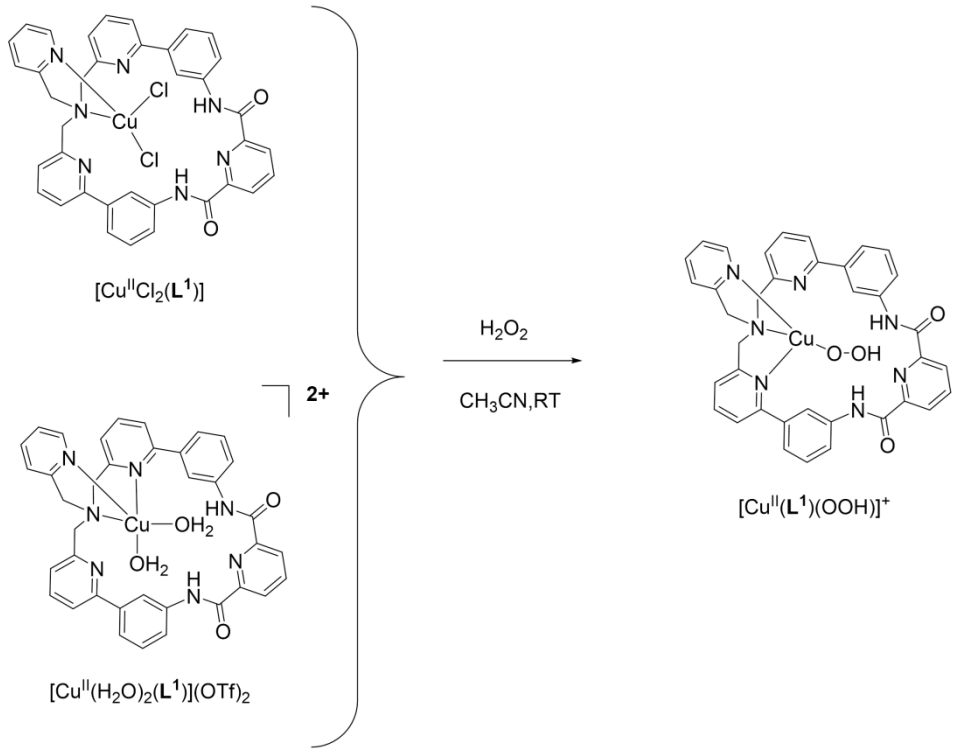

Scheme 4. Proposed reaction of complex **1** and **3** with H_2O_2 in acetonitrile, yielding the hydroperoxo species.

4. Conclusions

In summary, we have reported here the synthesis and characterization of three new mononuclear copper(II) complexes **1-3** bearing ditopic macrocyclic ligands (**L**^{1} or **L**^{2}). The solid state studies for **1** and **3** demonstrate that the Cu(II) ion is preferably coordinated in the TPA site, as previously found with the Fe(II)-**L**^{1} analogous complex [22]. However, the coordination sphere of the copper centre is dictated by the Cu(II) salt used for the synthesis, since the tetracoordinated complex **1** prefers a distorted square-planar geometry at solid state while the pentacoordinated complex **3** displays an almost perfect square-pyramidal conformation. When dissolved in acetonitrile, both complexes adopt a square-pyramidal geometry, as emphasized by EPR studies. Electrochemical studies of complexes **1** and **3** show a strong rearrangement of the coordination sphere upon electron transfer. Remarkably, the reaction of **1** or **3** with H_2O_2 yields a copper(II)-hydroperoxo species which is stable at room temperature. Future works will aim at studying the catalytic properties of the Cu^{II}-OOH species towards organic substrates, and in particular the possible HAT of aliphatic hydrogenated substrates through monoelectronic oxidation.

Acknowledgments

The authors acknowledge the Université de Bretagne Occidentale (UBO) for PhD grant (M. Ayad). Dr. Francois Michaud is thanked for X-Ray diffraction analysis. The Agence Nationale de la Recherche (ANR-11-BS07-0024) is thanked for financial support.

Supplementary information

Experimental and simulated EPR spectra, UV-Vis spectra and crystallographic data for complexes **1** and **3** (CCDC 1921004−1921005). Crystallographic data can be obtained free of charge via www.ccdc.cam.ac.uk/data_request/cif,or by emailing data_request@ccdc.cam.ac.uk, or by contacting The Cambridge Crystallographic Data Centre, 12 Union Road, Cambridge CB2 1EZ, UK; fax: +44 1223 336033.

References

[1] M. Sankaralingam, Y.-M. Lee, W. Nam, S. Fukuzumi, Coord. Chem. Rev., 365 (2018) 41-59.
[2] D.S. Nesterov, O.V. Nesterova, A.J.L. Pombeiro, Coord. Chem. Rev., 355 (2018) 199-222.
[3] C.E. Elwell, N.L. Gagnon, B.D. Neisen, D. Dhar, A.D. Spaeth, G.M. Yee, W.B. Tolman, Chem. Rev., 117 (2017) 2059-2107.
[4] E. Abad, J.B. Rommel, J. Kastner, J. Biol. Chem., 289 (2014) 13726-13738.
[5] D.A. Quist, D.E. Diaz, J.J. Liu, K.D. Karlin, J. Biol. Inorg. Chem., 22 (2017) 253-288.
[6] R.E. Cowley, L. Tian, E.I. Solomon, Proc. Natl. Acad. Sci. U. S. A., 113 (2016) 12035-12040.
[7] E.D. Hedegard, U. Ryde, J. Biol. Inorg. Chem., 22 (2017) 1029-1037.
[8] D.T. Yin, S. Urresti, M. Lafond, E.M. Johnston, F. Derikvand, L. Ciano, J.G. Berrin, B. Henrissat, P.H. Walton, G.J. Davies, H. Brumer, Nat. Commun., 6 (2015) 10197.
[9] M. Mahroof-Tahir, N.N. Murthy, K.D. Karlin, N.J. Blackburn, S.N. Shaikh, J. Zubieta, Inorg. Chem., 31 (1992) 3001-3003.

[10] A. Wada, M. Harata, K. Hasegawa, K. Jitsukawa, H. Masuda, M. Mukai, T. Kitagawa, H. Einaga, Angew. Chem. Int. Ed., 37 (1998) 798-799.
[11] M. Kodera, T. Kita, I. Miura, N. Nakayama, T. Kawata, K. Kano, S. Hirota, J. Am. Chem. Soc., 123 (2001) 7715-7716.
[12] T. Fujii, A. Naito, S. Yamaguchi, A. Wada, Y. Funahashi, K. Jitsukawa, S. Nagatomo, T. Kitagawa, H. Masuda, Chem. Commun., (2003) 2700.
[13] T. Fujii, S. Yamaguchi, Y. Funahashi, T. Ozawa, T. Tosha, T. Kitagawa, H. Masuda, Chem. Commun., (2006) 4428-4430.
[14] L. Li, A.A. Sarjeant, K.D. Karlin, Inorg. Chem., 45 (2006) 7160-7172.
[15] D. Maiti, H.R. Lucas, A.A. Sarjeant, K.D. Karlin, J. Am. Chem. Soc., 129 (2007) 6998-6999.
[16] D. Maiti, A.A. Sarjeant, K.D. Karlin, J. Am. Chem. Soc., 129 (2007) 6720-6721.
[17] A. Kunishita, M. Kubo, H. Ishimaru, T. Ogura, H. Sugimoto, S. Itoh, Inorg. Chem., 47 (2008) 12032-12039.
[18] Y.J. Choi, K.B. Cho, M. Kubo, T. Ogura, K.D. Karlin, J. Cho, W. Nam, Dalton Trans., 40 (2011) 2234-2241.
[19] S. Kim, C. Saracini, M.A. Siegler, N. Drichko, K.D. Karlin, Inorg. Chem., 51 (2012) 12603-12605.
[20] S. Biswas, A. Dutta, M. Debnath, M. Dolai, K.K. Das, M. Ali, Dalton Trans., 42 (2013) 13210-13219.
[21] N. Kindermann, S. Dechert, S. Demeshko, F. Meyer, J. Am .Chem. Soc., 137 (2015) 8002-8005.
[22] M. Ayad, R.J.M. Klein Gebbink, Y. Le Mest, P. Schollhammer, N. Le Poul, F.Y. Petillon, D. Mandon, Dalton Trans., 47 (2018) 15596-15612.
[23] X. Zhang, D. Huang, Y.S. Chen, R.H. Holm, Inorg. Chem., 51 (2012) 11017-11029.
[24] M. Ayad, Thesis, University of Brest (2017).
[25] G. Sheldrix, SHELXS 97, University of Gottingen, Germany (1997).
[26] L.J. Farrugia, J. Appl. Crystallogr., 32 (1999) 837-838.
[27] E.V. Rybak-Akimova, A.Y. Nazarenko, L. Chen, P.W. Krieger, A.M. Herrera, V.V. Tarasov, P.D. Robinson, Inorg. Chim. Acta, 324 (2001) 1-15.
[28] K.D. Karlin, J.C. Hayes, S. Juen, J.P. Hutchinson, J. Zubieta, Inorg. Chem., 21 (1982) 4106-4108.
[29] B.J. Hathaway, D.E. Billing, Coord. Chem. Rev., 5 (1970) 143-207.
[30] A. Kunishita, J. Teraoka, J.D. Scanlon, T. Matsumoto, M. Suzuki, C.J. Cramer, S. Itoh, J. Am. Chem. Soc., 129 (2007) 7248-7249.
[31] A.G.P. Gutierrez, J. Zeitouny, A. Gomila, B. Douziech, N. Cosquer, F. Conan, O. Reinaud, P. Hapiot, Y. Le Mest, C. Lagrost, N. Le Poul, Dalton Trans., 43 (2014) 6436-6445.
[32] D.B. Rorabacher, Chem. Rev., 104 (2004) 651-698.
[33] R.L. Peterson, J.W. Ginsbach, R.E. Cowley, M.F. Qayyum, R.A. Himes, M.A. Siegler, C.D. Moore, B. Hedman, K.O. Hodgson, S. Fukuzumi, E.I. Solomon, K.D. Karlin, J. Am. Chem. Soc., 135 (2013) 16454-16467.

TOC – graphical abstract